Molecules and Cells

PARP1 Impedes SIRT1-Mediated Autophagy during Degeneration of the Retinal Pigment Epithelium under Oxidative Stress

Ki-Hong Jang, Yeseong Hwang, and Eunhee Kim*

Department of Biological Sciences, Chungnam National University, Daejeon, Korea
*Correspondence: eunhee@cnu.ac.kr
https://doi.org/10.14348/molcells.2020.0078
www.molcells.org

The molecular mechanism underlying autophagy impairment in the retinal pigment epithelium (RPE) in dry age-related macular degeneration (AMD) is not yet clear. Based on the causative role of poly(ADP-ribose) polymerase 1 (PARP1) in RPE necrosis, this study examined whether PARP1 is involved in the autophagy impairment observed during dry AMD pathogenesis. We found that autophagy was downregulated following H_2O_2-induced PARP1 activation in ARPE-19 cells and olaparib, PARP1 inhibitor, preserved the autophagy process upon H_2O_2 exposure in ARPE-19 cells. These findings imply that PARP1 participates in the autophagy impairment upon oxidative stress in ARPE-19 cells. Furthermore, PARP1 inhibited autolysosome formation but did not affect autophagosome formation in H_2O_2-exposed ARPE-19 cells, demonstrating that PARP1 is responsible for impairment of late-stage autophagy in particular. Because PARP1 consumes NAD^+ while exerting its catalytic activity, we investigated whether PARP1 impedes autophagy mediated by sirtuin1 (SIRT1), which uses NAD^+ as its cofactor. A NAD^+ precursor restored autophagy and protected mitochondria in ARPE-19 cells by preserving SIRT1 activity upon H_2O_2. Moreover, olaparib failed to restore autophagy in SIRT1-depleted ARPE-19 cells, indicating that PARP1 inhibits autophagy through SIRT1 inhibition. Next, we further examined whether PARP1-induced autophagy impairment occurs in the retinas of dry AMD model mice. Histological analyses revealed that olaparib treatment protected mouse retinas against sodium iodate (SI) insult, but not in retinas cotreated with SI and wortmannin, an autophagy inhibitor. Collectively, our data demonstrate that PARP1-dependent inhibition of SIRT1 activity impedes autophagic survival of RPE cells, leading to retinal degeneration during dry AMD pathogenesis.

Keywords: autophagy, dry AMD, oxidative stress, PARP1, SIRT1

INTRODUCTION

Autophagy plays an important role in the protection of photoreceptors and neurosensory retinal cells by the retinal pigment epithelium (RPE) (Mitter et al., 2014). Consistently, autophagy is often compromised in dry age-related macular degeneration (AMD) patients (Kaarniranta et al., 2013; Mitter et al., 2014). Impaired autophagy leads to accumulation of damaged organelles, aggregation-prone proteins and drusen deposits, which is involved in dry AMD pathogenesis (Hyttinen et al., 2017; Kaarniranta et al., 2013). Therefore, proper regulation of autophagy is important for the prevention of dry AMD pathogenesis.

Autophagy participates in a degradative mechanism to eliminate impaired organelles and misfolded proteins (Cuervo et al., 2005; Kiffin et al., 2006; Nah et al., 2015; Navarro-Yepes et al., 2014). Various proteins are involved in the

Received 25 March, 2020; revised 23 May, 2020; accepted 5 June, 2020; published online 20 July, 2020

eISSN: 0219-1032

conjugation of phosphatidylethanolamine to microtubule-associated protein-light chain 3 (LC3), which modifies LC3. Modified LC3 (LC3-II) recruits p62, which conveys aggregated proteins to phagophores, and autophagosomes are formed (Ohsumi, 2001; Ryter et al., 2013). Eventually, the autophagosomes fuse with lysosomes, and the cargo proteins are subsequently degraded together with p62 (Ohsumi, 2001).

Poly(ADP-ribose) polymerase (PARP) 1 is a member of the PARP enzyme family, which catalyzes the transfer of ADP-ribose onto target proteins using NAD^+ (Abd Elmageed et al., 2012; Gibson and Kraus, 2012). Among the 17 PARP family members, PARP1 plays a key role in poly(ADP-ribose) (PAR)-mediated cellular physiology because > 95% of PARs are derived from PARP1 (Fatokun et al., 2014). However, PARP1 plays dual roles depending on the cellular context. PARP1 performs a protective function by recruiting repair proteins upon minor DNA damage (Gibson and Kraus, 2012). In contrast, overactivated PARP1 causes an energy crisis and leads to parthanatos, a regulated type of necrosis that occurs in response to extensive DNA damage (Galluzzi et al., 2018; Yetimakman et al., 2014).

During the parthanatos process, PARs bind to apoptosis-inducing factors (AIFs) in the mitochondrial outer membrane (Wang et al., 2011). Subsequently, the PAR-bound AIFs move to the nucleus and induce DNA fragmentation on a large scale, resulting in necrotic death in diverse cell types (David et al., 2009; Fatokun et al., 2014). However, our previous study showed that AIF does not move to the nucleus in the context of RPE death under oxidative stress even though PARP1 activation is essential (Jang et al., 2017). Furthermore, AIF is dispensable for the completing of PARP1-mediated RPE death, implying that a novel death mechanism distinct from the canonical parthanatos pathway might mediate oxidative stress-induced RPE death. This possibility led us to investigate downstream effectors of PARP1 distinct from members of the AIF-mediated pathway during RPE death.

Sirtuins (SIRTs), like PARPs, use cellular NAD^+ for their enzymatic activity. SIRTs are NAD^+-dependent histone/protein deacetylases encoded by genes homologous to the yeast silent information regulator 2 gene (Imai et al., 2000). Seven mammalian SIRTs are involved in metabolism, proliferation, inflammation, and autophagy (Chang and Guarente, 2014; Imai et al., 2000). In particular, SIRT1 is a key regulator of autophagy among SIRTs (Lee, 2019; Salminen and Kaarniranta, 2009). SIRT1 deacetylates diverse autophagy-related proteins, including autophagy-related gene (ATG) family members and LC3 (Hariharan et al., 2010; Huang and Liu, 2015; Huang et al., 2015; Lee et al., 2008). Furthermore, SIRT1 indirectly regulates autophagy by deacetylating transcription factors, increasing the expression of ATGs (Hu et al., 2016). Consistent with the disease relevance of autophagy, SIRT1 has been implicated in diverse diseases, including retinal degenerative disorders (Luo et al., 2019; Rubinsztein et al., 2011; Wu et al., 2011).

RPE cells are more resistant than other retinal cells to oxidative stress due to their high basal levels of autophagy (Golestaneh et al., 2017; Kurz et al., 2009; Lin and Xu, 2019). Therefore, impairment of autophagy sensitizes RPE cells to oxidative stress (Mitter et al., 2014). However, the molecular mechanism of autophagy impairment in RPE cells under the pathological conditions of dry AMD is not clear. Here, we investigated whether PARP1 is involved in autophagy impairment during oxidative stress-induced RPE degeneration. We found that PARP1 compromises late-stage autophagy via SIRT1 inactivation and subsequently leads to RPE degeneration in cellular and mouse models of dry AMD.

MATERIALS AND METHODS

Reagents and antibodies

Numerous reagents were purchased commercially. Bafilomycin A1, hydrogen peroxide, 3-methyl adenine, β-nicotinamide mononucleotide (β-NMN), chloroquine (CQ), wortmannin, sodium iodate (SI), 50% glutaraldehyde, rapamycin (RAPA), a rabbit anti-p62 antibody, and a mouse β-actin antibody were purchased from Sigma-Aldrich (USA); a horseradish peroxidase (HRP)-conjugated anti-mouse antibody, a HRP-conjugated anti-rabbit antibody, a fluorescein-conjugated anti-mouse antibody and 4′,6-diamidino-2-phenylindole (DAPI) were purchased from Thermo Fisher Scientific (USA); a mouse anti-PARP1 antibody was purchased from BD Biosciences (USA); rabbit anti-LC3, anti-lysosomal-associated membrane protein (LAMP1), anti-phospho mammalian target of rapamycin (mTOR) (serine 2248), anti-mTOR, and anti-acetyl p53 (lysine 382) antibodies were purchased from Cell Signaling Technology (USA); rabbit anti-AIF, mouse anti-p53, and mouse anti-RPE65 antibodies were purchased from Santa Cruz Biotechnology (USA); a mouse anti-PAR antibody was purchased from Enzo Life Sciences (USA) and Abcam (England); and olaparib was purchased from Selleck Chemicals (USA).

Cell culture

Human cultured retinal pigment epithelium (ARPE-19) cells were cultured in Dulbecco's modified Eagle's medium (DMEM; WelGENE, Korea)/F12 supplemented with 10% fetal bovine serum (Atlas Biologicals, USA) and 1% penicillin/streptomycin (Thermo Fisher Scientific) at 37°C in a 5% CO_2 atmosphere.

Plasmids

The LC3 constructs tandemly tagged with red fluorescent protein (RFP) and green fluorescent protein (GFP) (RFP-GFP-LC3) were kindly provided by Dr. KS Kwon (Korea Bioscience and Biotechnology, Korea). The vector pDsRed-Mito-MTS was purchased from Clontech Laboratories (USA) to visualize mitochondria.

Flow cytometry

ARPE-19 cells were treated with 0.1 mM or 0.5 mM H_2O_2 for the indicated times. The cells were then harvested and stained with propidium iodide at a final concentration of 5 μg/ml. In another set of experiments, ARPE-19 cells were treated with 0.5 mM H_2O_2 or 100 μM CQ for 6 h and then with 2.5 μM LysoTracker Red DND-99 for 10 min to measure lysosomal morphology. The red color intensity was measured using a Guava easyCyte flow cytometer (Millipore, Germany).

Gene silencing

Small interfering RNA (siRNA) oligonucleotides were purchased from Bioneer (Korea) with sequences targeting ATG7 (5′-CAGCUAUUGGAACACUGUA-3′), SIRT1 (5′-CUGUGAAAUUACUGCAAGA-3′), and AIF (5′-GCAAGUUACUUAUCAAGCU-3′). ARPE-19 cells were transfected with 200 nM of the indicated siRNA or scrambled RNA (scRNA) using Lipofectamine RNAiMAX reagent (Thermo Fisher Scientific) according to the manufacturer's instructions. The effects of siRNA on the indicated protein levels were examined by western blot analysis.

Fluorescence and immunofluorescence

ARPE-19 cells were transiently transfected with RFP-GFP-LC3 or DsRed-Mito (Clontech Laboratories). After 48 h of transfection, the ARPE-19 cells were treated with 0.5 mM H_2O_2 in the presence or absence of the indicated compounds. The cells were fixed with 4% paraformaldehyde for 15 min, and the nuclei were stained with DAPI for 10 min. For immunofluorescence, ARPE-19 cells transfected with GFP-LC3 were treated with 0.5 mM H_2O_2 for 1 h. The cells were then fixed with 4% paraformaldehyde and permeabilized with 0.01% Triton X-100 for 10 min before being were incubated with an anti-LAMP-1 antibody overnight at 4°C and then washed three times with phosphate-buffered saline (PBS). Solutions of fluorescent dye-conjugated secondary antibodies were added to the cells, which were incubated for 2 h at room temperature, and the nuclei were stained with DAPI. Coverslips for all samples were mounted onto microscope slides using fluorescence mounting medium (Agilent Technologies, USA). All samples were analyzed using a Zeiss LSM 510 laser scanning confocal microscope (Carl Zeiss, Germany).

Western blot analysis

ARPE-19 cells were lysed in lysis buffer (20 mM Tris-HCl pH 7.5 containing 150 mM NaCl, 2 mM EDTA, 1% NP-40, 0.4 mM PMSF, 25 mM β-glycerophosphate, 1 mM Na_3VO_4, 1 mM DTT, and 1 mM NaF) and then centrifuged at 12,000*g* for 10 min at 4°C. The protein concentrations were determined by the Bradford method using a Bio-Rad protein assay kit (Bio-Rad, USA). The samples were separated by SDS-PAGE and transferred to nitrocellulose membranes. The membranes were blocked with 5% skim milk and incubated with the indicated primary antibodies at 4°C for 12 h. After three washes for 10 min each, the membranes were incubated with HRP-conjugated secondary anti- mouse or anti-rabbit antibodies. The protein bands were visualized using an enhanced chemiluminescence detection kit (YounginFrontier, Korea).

Measurement of lysosomal pH

ARPE-19 cells were seeded into 96-well plates (1×10^4 cells/well) and incubated for 12 h. The cells were treated with 0.5 mM H_2O_2 and then incubated with 10 μM LysoSensor Yellow/Blue DND-160 dye for 10 min in a 37°C CO_2 incubator. A standard curve was obtained with ARPE-19 cells treated with 10 μM monensin and nigericin in MES buffer (5 mM NaCl, 115 mM KCl, 25 mM 2-(N-morpholino)ethanesulfonic acid, and 1.3 mM $MgSO_4$). The samples were then measured with a VICTOR microplate reader (PerkinElmer, USA).

Measurement of mitochondrial membrane potential

ARPE-19 cells were treated with 0.5 mM H_2O_2 in the presence or absence of 100 μM β-NMN and wortmannin for 3 h, and then harvested. Mitochondrial membrane depolarization was measured using a Muse MitoPotential Kit (Millipore). Briefly, cells were incubated with Muse MitoPotential dye for 20 min in a 37°C CO_2 incubator. Subsequently, changes in mitochondrial membrane potential were determined with a Muse analyzer (Millipore).

Measurement of intracellular NAD^+ and ATP levels

ARPE-19 cells were seeded into 96-well plates (1×10^4 cells/well) and incubated for 12 h. The cells then were then treated with 0.5 mM H_2O_2 in the presence or absence of 10 μM olaparib for 4 h. The cellular NAD^+ levels were measured using a NAD/NADH-Glo assay kit (Promega, USA) and ATP levels were measured using the CellTiter-Glo vability assay kit (Promega) according to the manufacturer's instructions.

Animal model

C57BL/6 mice (male, 10-12 weeks old, weight range 26-28 g) were purchased from Central Lab Animal (Korea). All mice were maintained in the animal facility of Chungnam National University (Korea) and acclimatized to a light schedule of alternating 12-h periods of light and dark with free access to food and water for at least 1 week before the experiment, and these conditions were maintained through the experiment. All animal studies were approved (201906A-CNU-091) and conducted in accordance with the institutional guidelines for the care and use of laboratory animals. After 7 days of acclimation, the mice were randomly divided into groups that were anlyzed 0, 0.5, 1, 2, 4, and 7 days after 30 mg/kg SI injection. The mice were divided into the following groups (n = 3 per group) and treated by intraperitoneal (i.p.) injection: a control group, a vehicle-olaparib (15 mg/kg, i.p.) group, an SI-vehicle group and an SI-olaparib group. Two days after SI injection, protein lysates from the retinas of the mice were used for western blot analysis. To evaluate the protective effect of olaparib, mice were randomly divided into control, vehicle-olaparib, vehicle-olaparib-wortmannin (1 mg/kg, i.p.), SI-vehicle, SI-olaparib, and SI-olaparib-wortmanin groups (n = 3 per group). Five days after SI injection, the retinas of the mice were used for morphological analysis by H&E staining.

Protein extraction from mouse retinas

RPE cells and retinas were separated from enucleated mouse eyes according to previously described (Wei et al., 2016). Briefly, the retinas were removed elucidated mouse eyes. The RPE/choroid/sclera were placed in protein lysis buffer for 1 h and then choroid/sclera were removed. Then the RPE cells were incubated at 4°C and the retinas were homogenized in lysis buffer, and the homogenates were centrifuged at 12,000*g* for 10 min at 4°C. The total protein concentrations were measured by the Bradford method. Equal amounts of protein were subjected to western blot analysis.

H&E staining

Enucleated mouse eyes were prefixed in 4% glutaraldehyde in PBS at room temperature for 20 min, and the lenses were

removed. Next, the samples were incubated in 4% glutaraldehyde in PBS for 12 h at 4°C and embedded using routine procedures. After embedding, retinal cross sections were prepared with a thickness of 5 μm. The slices were dewaxed, stained with hematoxylin for 4 min, and restained with eosin for 1 min. The samples were observed under an optical microscope (Leica Microsystems, Germany) and imaged with a slide scanner (Motic Electronic, China).

Statistical analyses

At least 3 independent replicates were examined for the *in vitro* and *in vivo* experiments. All data are expressed as the mean ± SD. The statistical significance of differences between the experimental and control groups was evaluated by performing two-tailed *t*-test using IBM SPSS Statistics (ver. 22; IBM, USA). *P* values less than 0.05 were considered significance.

RESULTS

H_2O_2 induces PARP1 activation and compromises autophagy in ARPE-19 cells

PARP1-mediated necrosis is responsible for a substantial portion of the RPE death elicited by oxidative stress (Jang et al., 2017). Compromised autophagy is also known to contribute to RPE death under oxidative stress (Mitter et al., 2014). This led us to investigate whether PARP1 activation is related to autophagy impairment in RPE death upon oxidative stress. To this end, we treated ARPE-19 cells with two concentrations of H_2O_2. H_2O_2 at 0.1 mM did not change the death of ARPE-19 cells (Fig. 1A) and alter the LC3-II/-I ratio (Fig. 1B). In contrast, 0.5 mM H_2O_2 led to cell death following PARP1 activation and elevated the LC3-II/-I ratio (Figs. 1A and 1B). To understand the mechanism underlying the elevation in the LC3-II/-I ratio mediated by 0.5 mM H_2O_2, we used early-stage and late-stage autophagy inhibitors (3-methyladenine [3-MA] and bafilomycin A1 [BafA1], respectively). Hereafter, "H_2O_2" refers to 0.5 mM H_2O_2 unless stated otherwise. BafA1 increased the LC3-II/I ratio, demonstrating the integrity of the autophagy machinery in ARPE-19 cells (Fig. 1C). However, 3-MA suppressed the conversion of LC3-I into LC3-II when used in combination with H_2O_2. In contrast, H_2O_2 treatment did not affect the BafA1-induced conversion of LC-I into LC3-II (Fig. 1C). This indicates that H_2O_2 did not induce LC3-II conversion by autophagy activation but rather led to LC3-II accumulation through inhibition of the degenerative pathway in autophagy.

To further confirm that H_2O_2 inhibits late-stage autophagy, we examined subcellular localization-dependent changes in the fluorescence of RFP-GFP-LC3 (Fig. 1D). RFP-GFP-LC3 emits both red and green fluorescence signals and appears as yellow in merged images within autophagosomes. However, RFP-GFP-LC3 is visualized as red fluorescent vesicles in acidic environments like autolysosomes by GFP quenching (Yoshii and Mizushima, 2017). The number of red fluorescent vesicles increased upon RAPA treatment, showing that autophagy was properly induced in ARPE-19 cells. In addition, the number of yellow fluorescent vesicles increased in ARPE-19 cells treated with BafA1 as well as H_2O_2, demonstrating the accumulation of nonacidified autophagosomes. This accumulation have been due to either neutralization of lysosomal pH or impaired fusion of autophagosomes with lysosomes. To discriminate between these two possibilities, we first measured the lysosomal pH upon H_2O_2 treatment. The lysosomal pH of ARPE-19 cells remained normal (pH 4.45 ± 0.045) in response to H_2O_2 (Supplementary Fig. S1A). We also investigated lysosomal integrity using LysoTracker Red DND-99. Chloroquine (CQ) treatment enlarged lysosomes and intensified the color of LysoTracker Red DND-99, indicating impairment of lysosomal integrity in ARPE-19 cells. However, the color intensity of LysoTracker Red DND-99 was equivalent between H_2O_2-treated and non-H_2O_2-treated ARPE-19 cells (Supplementary Fig. S1B), indicating that H_2O_2 did not affect lysosomal structures in ARPE-19 cells. These data indicate that neutralization of lysosomal pH did not happen in H_2O_2-treated ARPE-19 cells. Next, we investigated whether H_2O_2 affects the fusion of autophagosomes with lysosomes in ARPE-19 cells. Autophagosomes were represented with green fluorescence after GFP-LC3 transfection, and lysosomes were stained red by an anti-lysosomal-associated membrane protein1 (LAMP1) antibody. The numbers of yellow speckles representing colocalizations of LC3 with LAMP1 decreased upon H_2O_2 treatment in ARPE-19 cells, revealing that H_2O_2 compromised fusion of autophagosomes and lysosomes (Supplementary Fig. S1C). Collectively, our data demonstrate that H_2O_2 induces PARP1 activation and impairs the autophagy degenerative pathway in ARPE-19 cells, specifically the autophagosome-lysosome fusion process.

PARP1 suppresses autophagy in response to H_2O_2 in ARPE-19 cells

Because PARP1 activation precedes autophagy impairment in response to H_2O_2 (Fig. 1B), we examined whether a causal relationship exists between PARP1 activation and autophagy impairment. Pharmacological inhibition of PARP1 with olaparib did not alter the LC3-II/I ratio but decreased p62 expression in H_2O_2-treated ARPE-19 cells (Fig. 2A). Furthermore, the p62 turnover induced by olaparib was blocked by knockdown of ATG7 using the siRNA system in H_2O_2-treated ARPE-19 cells (Fig. 2B). This implies that interference with PARP1 activation restores the autophagy process impaired by H_2O_2. Conversely, we investigated whether autophagy impairment affects PARP1 activity under oxidative stress. Knockdown of ATG7 decreased p62 expression and the LC3-II/I ratio in the presence of H_2O_2, indicating that autophagy downregulation occurred at an early stage (Fig. 2C). However, PARP1 activity was maintained upon ATG7 silencing in H_2O_2-treated ARPE-19 cells, demonstrating that autophagy impairment does not affect PARP1 activity (Fig. 2C).

To further validate that PARP1 impairs autophagy, we examined the subcellular localizations of LC3 using RFP-GFP-LC3. Upon H_2O_2 treatment, the number of yellow fluorescent vesicles increased, demonstrating failure of autolysosome formation (Fig. 2D). However, olaparib treatment increased the number of red fluorescent puncta while decreasing the number of yellow vesicles in H_2O_2-treated ARPE-19 cells, indicating that inhibition of PARP1 enzyme activity restored autophagy (Fig. 2D).

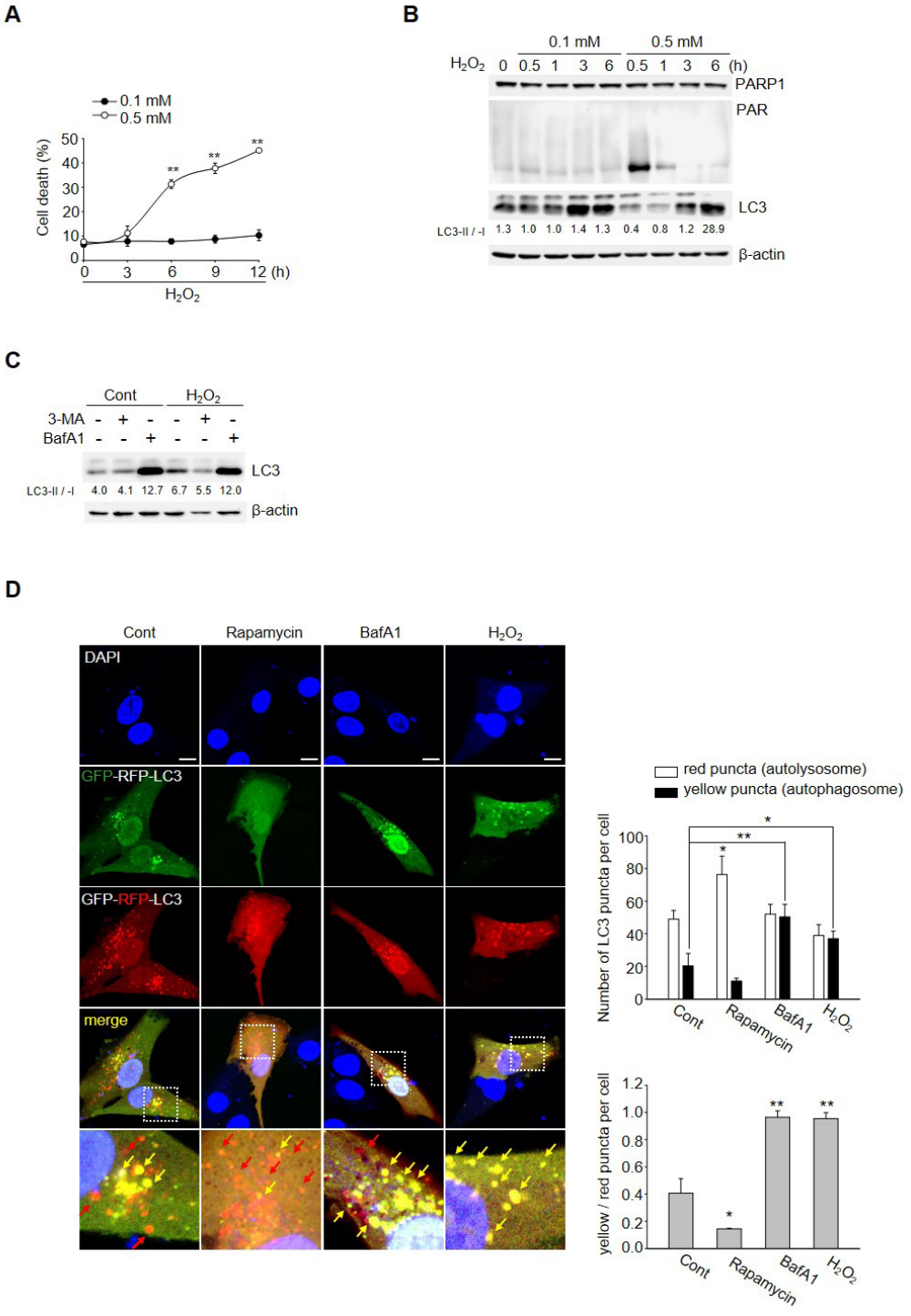

Fig. 1. H_2O_2 induces PARP1 activation and compromises autophagy in ARPE-19 cells. (A and B) ARPE-19 cells were treated with 0.1 mM or 0.5 mM H_2O_2 for the indicated times. (A) Cell death was analyzed by flow cytometry using propidium iodide staining. (B) The cell lysates were immunoblotted with the indicated antibodies. (C) ARPE-19 cells were treated with 0.5 mM H_2O_2 in the presence or absence of the autophagy inhibitors 3-methyladenine (3-MA, 10 μM) and bafilomycin A1 (BafA1, 100 nM). The cell lysates were immunoblotted with the indicated antibodies. Cont, control. (B and C) LC3-II/-I ratio was quantified by densitometric analyses. (D) ARPE-19 cells were transfected with RFP-GFP-LC3 and seeded on poly-D-lysine-coated coverslips. Next, the cells were treated with 0.5 mM H_2O_2 or autophagy modulators (inducer: rapamycin, 100 nM, or inhibitor: BafA1, 100 nM) for 6 h. The nuclei were stained with 4′,6-diamidino-2-phenylindole (DAPI). Red and yellow arrows indicate autolysosomes and autophagosomes, respectively. Scale bars = 10 μm. (A and D) Quantified data are expressed as the mean ± SD from three independent biological replicates. Statistical analysis was performed by Student's *t*-test. $*P < 0.05$, $**P < 0.01$.

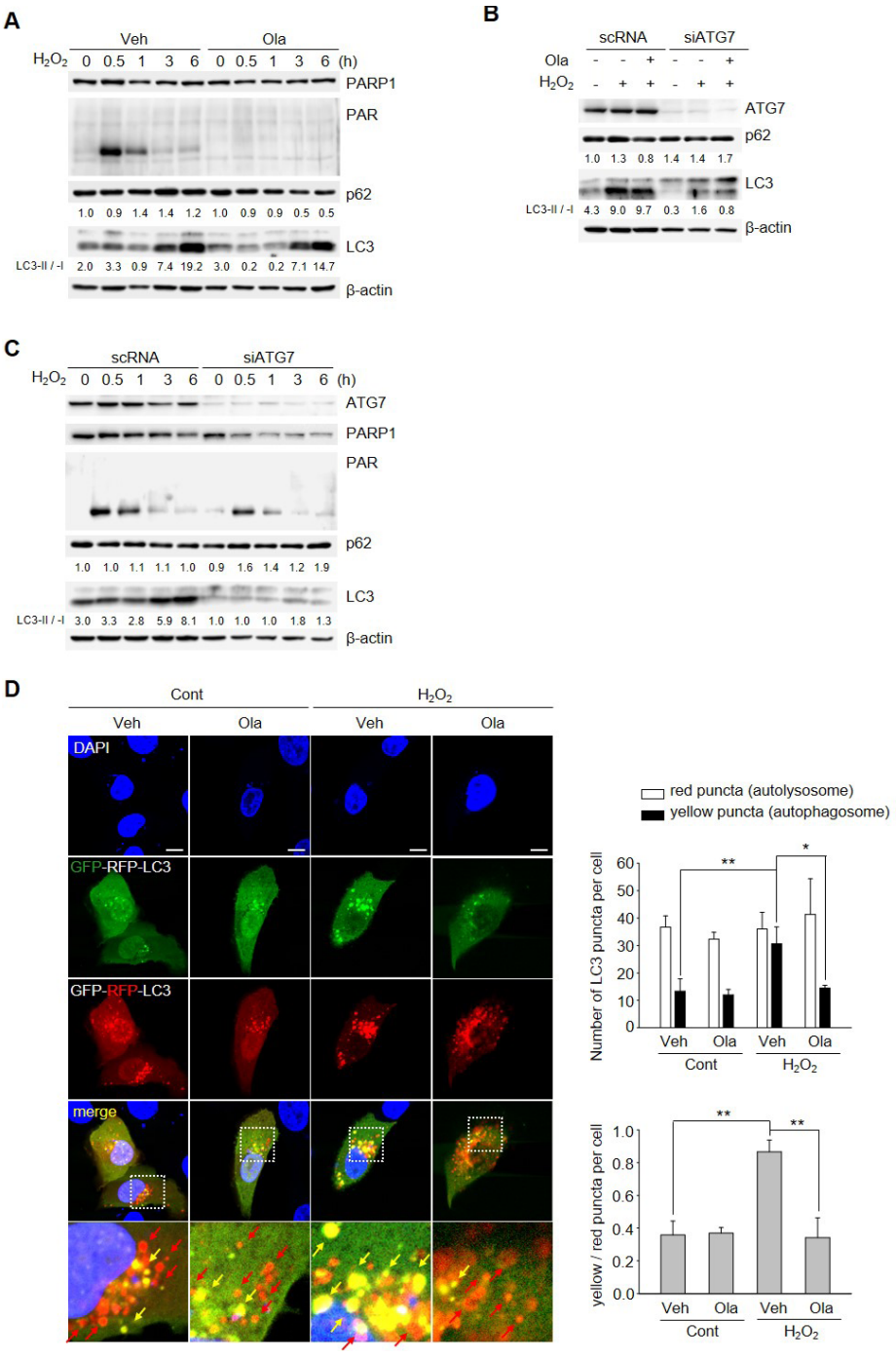

Fig. 2. PARP1 suppresses autophagy in response to H_2O_2 in ARPE-19 cells. (A) ARPE-19 cells were treated with 0.5 mM H_2O_2 for the indicated times in the presence or absence of 10 μM olaparib (Ola). Veh, vehicle. (B and C) ARPE-19 cells were transfected with scrambled siRNA (scRNA) or ATG7 targeting siRNA for 48 h. Then, the cells were treated with 0.5 mM H_2O_2 for 6 h in the presence or absence of 10 μM olaparib (B) for indicated times (C). (D and F) ARPE-19 cells were transfected with RFP-GFP-LC3 and seeded on poly-D-lysine-coated coverslips. Next, the cells were treated with 0.5 mM H_2O_2 for 6 h in the presence or absence of 10 μM olaparib (D) or pretreated with 100 μM rapamycin and then treated with 0.5 mM H_2O_2 for 6 h in the presence or absence of 10 μM olaparib (F). Nuclei were stained with 4′,6-diamidino-2-phenylindole (DAPI). Red and yellow arrows indicate autolysosomes and autophagosomes, respectively. Cont, control. Scale bars = 10 μm. (E and F) ARPE-19 cells were pretreated with 100 μM rapamycin for 5 h and then treated with 0.5 mM H_2O_2 for 1 h in the presence or absence of 10 μM olaparib. (A, B, C, and E) The cell lysates were immunoblotted with the indicated antibodies. The LC3-II/-I ratio and relative p62 levels were quantified by densitometric analyses (ImageJ software). (D and F) Quantified data are expressed as the mean ± SD from three independent biological replicates. Statistical analysis was performed by Student's *t*-test. $*P < 0.05$, $**P < 0.01$, $***P < 0.001$.

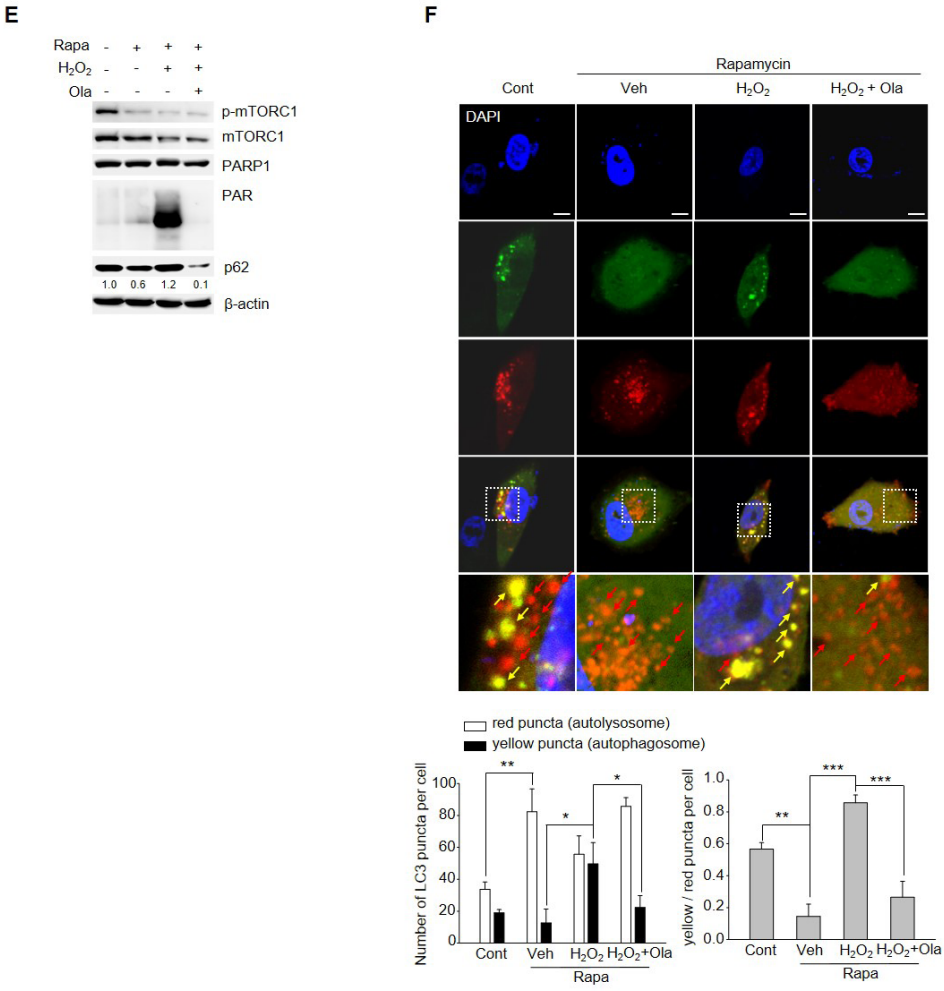

Fig. 2. Continued.

Next, we examined whether PARP1 can also negatively regulate pharmacologically activated autophagy in ARPE-19 cells. To this end, RAPA was used to activate autophagy in ARPE-19 cells. RAPA treatment decreased p62 levels but did not alter PARP1 activity in ARPE-19 cells. However, H_2O_2 treatment inhibited p62 turnover and activated PARP1 in RAPA-treated ARPE-19 cells. Olaparib restored p62 turnover in ARPE-19 cells cotreated with H_2O_2 and RAPA (Fig. 2E). These data imply that PARP1 activation by H_2O_2 also compromises RAPA-induced autophagy in ARPE-19 cells. Consistently, fluorescence data obtained using RFP-GFP-LC3 showed that PARP1 suppressed RAPA-induced autophagy in the late-stage upon H_2O_2 treatment (Fig. 2F). Taken together, these data demonstrate that a causal relationship is present between PARP1 and autophagy impairment, specifically PARP1 inhibits the late-stage of autophagy upon H_2O_2 treatment in ARPE-19 cells.

PARP1 suppresses autophagy via SIRT1 inhibition upon H_2O_2 treatment in ARPE-19 cells

Because AIF, a well-known downstream effector of PARP1 in parthanatos, is dispensable in the execution of H_2O_2-induced ARPE-19 cell death (Jang et al., 2017), we investigated the downstream effector(s) of PARP1 during the autophagy impairment process under oxidative stress. First, we examined whether AIF plays any role in the autophagy impairment process upon H_2O_2 treatment in ARPE-19 cells. Depletion of AIF using siRNA did not influence the extent of autophagy impairment in H_2O_2-treated ARPE-19 cells, indicating that AIF is dispensable for autophagy impairment as well as for death (Supplementary Fig. S2). This finding led us to look for other effectors. Considering that both PARP1 and SIRT1 need cellular NAD^+ for their activities, we examined whether PARP1 and SIRT1 interplay to acquire NAD^+ during the autophagy process (Luna et al., 2013). H_2O_2 treatment induced p53 acetylation, and NAD^+ replenishment decreased the acetylation status of p53, indicating that SIRT1 was inactivated upon H_2O_2 treatment in ARPE-19 cells (Fig. 3A). In contrast, olaparib blocked PAR production but activated SIRT1 via preserving NAD^+ levels upon H_2O_2 treatment (Supplementary Figs. S3A and S3B), implying that PARP1 interferes with SIRT1 activation. However, PARP1 activity was not altered in ARPE-

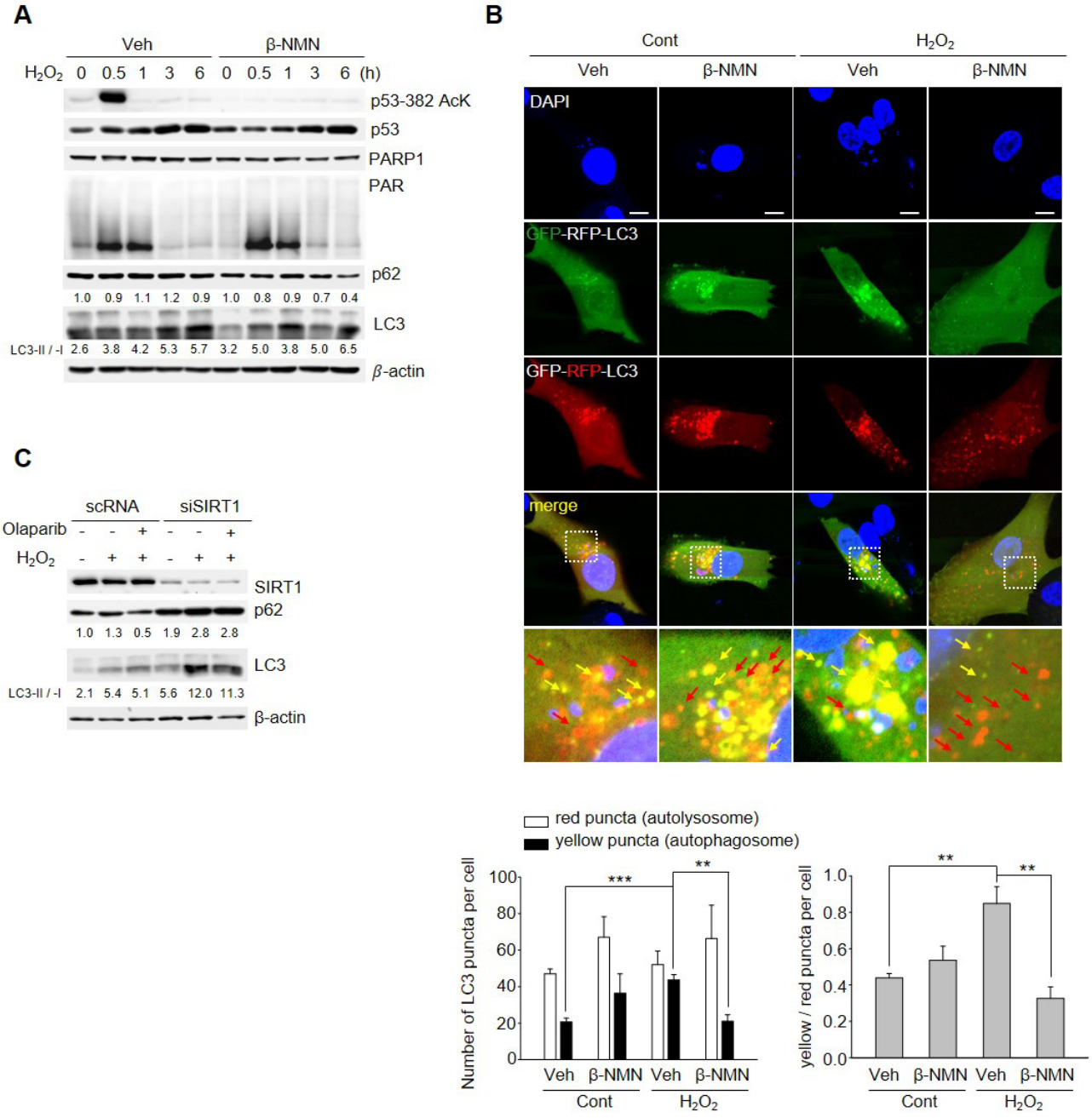

Fig. 3. PARP1 downregulates autophagy via SIRT1 inhibition under H_2O_2 treatment in ARPE-19 cells. (A and B) ARPE-19 cells were treated with H_2O_2 for the indicated times (A) or for 6 h in the presence or absence of 100 μM β-nicotinamide mononucleotide (β-NMN) (B). Cont, control; Veh, vehicle. Scale bars = 10 μm. (B) ARPE-19 cells were transfected with RFP-GFP-LC3 and then seeded on poly-D-lysine-coated coverslips. Subsequently, the cells were treated with 0.5 mM H_2O_2 for 6 h in the presence or absence of 100 μM β-NMN. The nuclei were stained with 4′,6-diamidino-2-phenylindole (DAPI). Red and yellow arrows indicate autolysosomes and autophagosomes, respectively. (A and C) The cell lysates were immunoblotted with the indicated antibodies. The LC3-II/-I ratio and relative p62 levels were quantified by densitometric analyses (ImageJ software). (B) Quantified data are expressed as the mean ± SD from three independent biological replicates. Statistical analysis was performed by Student's *t*-test. $^{**}P < 0.01$, $^{***}P < 0.001$.

19 cells cotreated with H_2O_2 and NAD^+ (Fig. 3A). Collectively, our data lead to conclude that SIRT1 acts downstream of PARP1. Next, we investigated whether the PARP1-SIRT1 axis regulates autophagy in ARPE-19 cells under H_2O_2 treatment. Upon NAD^+ replenishment in H_2O_2-treated ARPE-19 cells, p62 decreased, but the LC3-II/I ratio increased (Fig. 3A), indicating that autophagy was restored. Consistently, fluorescence data obtained using RFP-GFP-LC3 also showed that autophagy was restored by SIRT1 activation upon H_2O_2 treatment (Fig. 3B). Furthermore, olaparib treatment did not af-

fect autophagy flux under H_2O_2 treatment in SIRT1-depleted ARPE-19 cells, demonstrating that olaparib restores autophagy through preservation of SIRT1 activity in response to H_2O_2 (Fig. 3C). Together, these data show that PARP1-mediated SIRT1 inactivation impedes autophagy upon H_2O_2 treatment in ARPE-19 cells.

The PARP1-SIRT1 axis participates in mitochondrial dysfunction upon H_2O_2 treatment in ARPE-19 cells

Our previous finding that PARP1 leads to mitochondrial dysfunction upon H_2O_2 treatment in ARPE-19 cells (Jang et al., 2017) prompted us to investigate whether the PARP1-SIRT1 axis also operates during H_2O_2-mediated mitochondrial dysfunction. First, we measured mitochondrial depolarization in ARPE-19 cells under H_2O_2 treatment using a Muse analyzer. Mitochondrial depolarization of ARPE-19 cells increased to 35.5% ± 4.2% in response to H_2O_2 treatment (Figs. 4A and 4B). Fluorescence images also revealed the accumulation of damaged mitochondria in ARPE-19 cells subjected to H_2O_2 treatment, exhibiting disrupted mitochondrial morphology and increased mitochondrial fission (Figs. 4C and 4D). However, NAD^+ replenishment restored mitochondrial polarization levels in H_2O_2-exposed ARPE-19 cells (Figs. 4A and 4B). Furthermore, NAD^+ treatment preserved mitochondrial morphology and reduced mitochondrial fission upon H_2O_2 treatment in ARPE-19 cells (Figs. 4C and 4D). Finally, we measured intracellular ATP level following exposure to H_2O_2. ATP decreased to 39.5% ± 4.2% in response to H_2O_2, and the decrease was prevented by NAD^+ addition in ARPE-19 cells (Fig. 4E). Collectively, our findings demonstrate that that PARP1-SIRT1 axis operates in mitochondrial dysfunction under H_2O_2 treatment in ARPE-19 cells.

Autophagy compromise mediated by PARP1 elicits RPE degeneration in a dry AMD mouse model

Here, we aimed to validate that the RPE degeneration caused by PARP1-mediated autophagy impairment shown in H_2O_2-treated ARPE-19 cells also occurred in an *in vivo* model of dry AMD. To elicit oxidative stress in retinas, SI was administered to mice via intraperitoneal injection. We first examined PARP1 activity and analyzed autophagy upon SI treatment in the RPE cells and retinas of mice. PARs increased starting at 12 h, and these increases were sustained until 2 days after SI treatment. The p62 and LC3-II/I ratio also increased from 12 h, and these increases were sustained until 4 days after SI injection, demonstrating autophagy impairment (Fig. 5A). These data suggest that PARP1 activation might impair autophagy in retinas upon oxidative stress. To further address this issue, we treated SI-injected mice with olaparib via intraperitoneal injection. Olaparib treatment restored autophagy via preservation of SIRT1 activity in both RPE cells and retinas of SI-treated mice (Fig. 5B). We next measured morphological changes in retinas under SI treatment with or without olaparib treatment. Olaparib protected retinas against SI-induced oxidative damage (Figs. 5C and 5D), consistent with the findings of our previous study (Jang et al., 2017). Notably, olaparib treatment prevented discontinuity of RPE layer indicating RPE cell death in SI-injected mice (Fig. 5C, black arrows). However, this protective effect of olaparib was compromised when SI-injected mice were cotreated with wortmannin, an autophagy inhibitor, in addition to olaparib (Figs. 5C and 5D). This finding indicates that PARP1 attenuates autophagy and causes accompanying retinal morphological alterations under conditions of oxidative stress. Taken together, our findings demonstrate that PARP1 leads to retinal degeneration via autophagy impairment in dry AMD mouse model.

DISCUSSION

In this study, we elucidated the molecular mechanism underlying autophagy impairment during RPE degeneration in response to oxidative stress: activated PARP1 impeded the degenerative pathway of autophagy via SIRT1 inhibition upon oxidative stress. This process represented the PARP1-SIRT1 axis. Furthermore, the PARP1-SIRT1 axis led to mitochondrial dysfunction in RPE cells subjected to oxidative stress. Such autophagy impairment through PARP1-SIRT1 interplay was also shown to cause RPE degeneration in a dry AMD mouse model using SI. Taken together, our data reveal a novel role of PARP1 in promoting dry AMD pathogenesis as an autophagy suppressor in addition to its previously identified role as a parthanatos trigger.

Apparent discrepancy regarding autophagy mechanism between this study and previous ones seems to come from characteristics of stress. For example, prolonged exposure to sublethal H_2O_2 impairs autophagy in early stage with reduced expression of Beclin-1, ATG7 and 9 in RPE cells (Mitter et al., 2014). In contrast, our study showed that exposure to lethal H_2O_2 compromises autophagy in late stage with differential activations of PARP1 and SIRT1 in RPE cells. Similarly, cigarette smoking extract-induced oxidative stress leading to RPE death also compromised autophagy in late stage (Govindaraju et al., 2017). Collectively, these findings imply that autophagy impairment in RPE cells could be derived from distinctive mechanisms depending on duration, concentration and type of stress. Such differential blocking mechanisms against autophagy process depending on the stress characteristics have been also shown in neurodegenerative disease (Menzies et al., 2017).

The literature shows that PARP1 often exerts positive effects on autophagy. For example, PARP1 promotes autophagy at the initiation stage, triggering autophagosome formation via parylation of AMP-activated protein kinase upon starvation in mouse embryonic fibroblasts (MEFs) (Rodriguez-Vargas et al., 2016; 2019; Wang et al., 2018). In addition, PARP1 facilitates autophagy by shuttling DNA repair proteins to the nucleoplasm and increasing genomic stability in macrophages inflammatory response conditions (Ke et al., 2017). These findings contrast with the suppressive role of PARP1 in oxidative stress-exposed RPE cells revealed in this study. PARP1 also inhibits late-stage autophagy in MEFs under oxidative stress (Wyrsch et al., 2012). Collectively, the data seem to be indicate that PARP1 functions as a multifaceted regulator in different stages of autophagy depending on the stimulus and cellular context.

PARP1 functions upstream of SIRT1 in dry AMD, as shown in this study. Furthermore, PARP1 suppresses SIRT1 activity in other diseases related to muscles and neurons (Bai et al.,

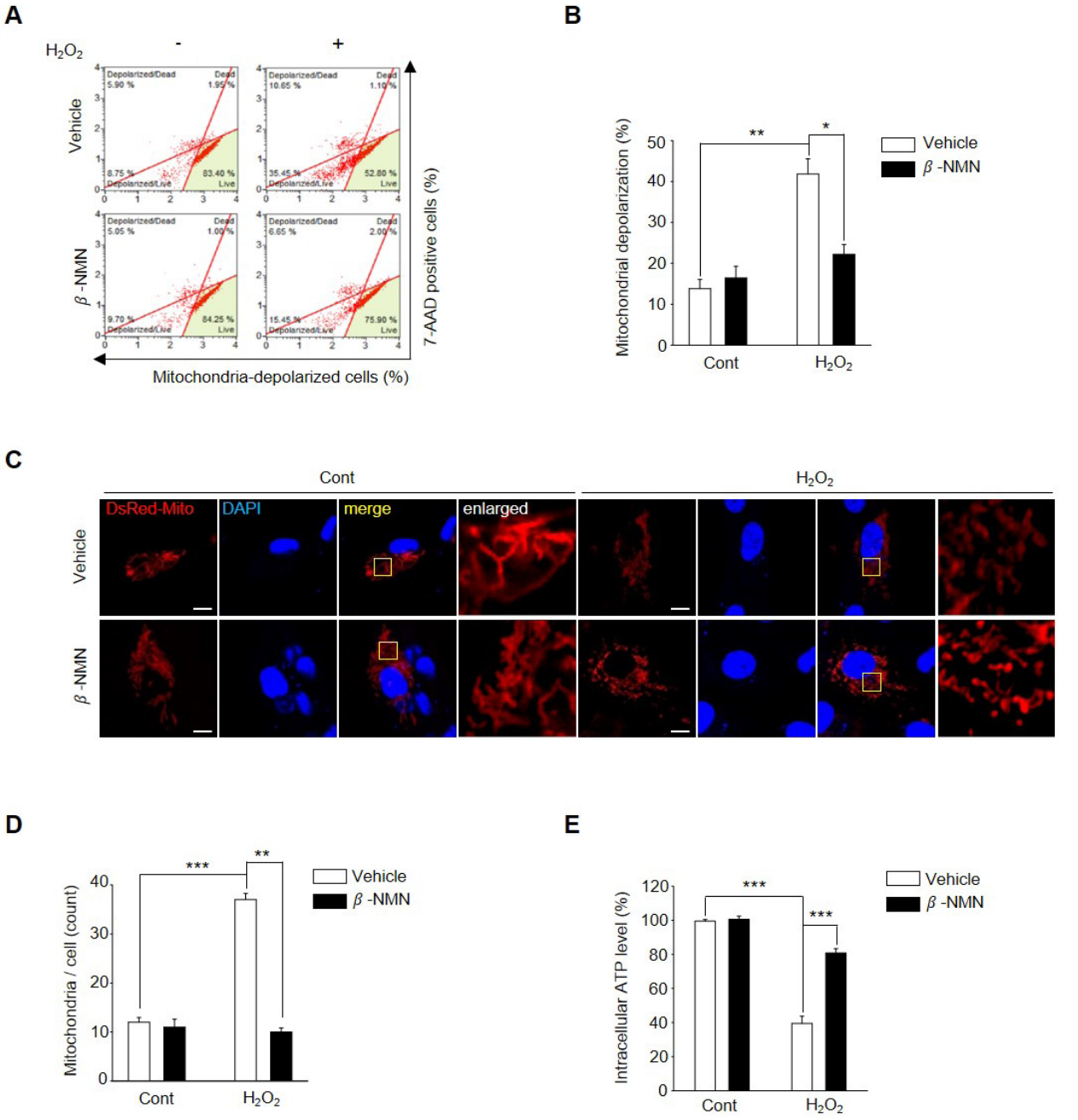

Fig. 4. The PARP1-SIRT1 axis participates in mitochondrial dysfunction upon H_2O_2 treatment in ARPE-19 cells. (A and E) ARPE-19 cells were treated with 0.5 mM H_2O_2 in the presence or absence of 100 μM β-nicotinamide mononucleotide (β-NMN) for 3 h. Then, the mitochondrial membrane potential of the cells was measured using a Muse analyzer (A) or intracellular ATP using a VICTOR plate reader (E). The cells in the left quadrant are depolarized cells. (B) The graph was obtained from a quantitative analysis of depolarized cells. (C) ARPE-19 cells were transfected with DsRed-Mito to observe mitochondrial morphology (red) for 48 h and seeded on poly-D-lysine-coated coverslips. Subsequently, the cells were treated with 0.5 mM H_2O_2 in the presence or absence of 100 μM β-NMN for 1 h. The nuclei were visualized by 4′,6-diamidino-2-phenylindole (DAPI) staining. Cont, control. Scale bars = 10 μm. (D) The graph shows the numbers of fragmented mitochondria per cells (n ≥ 10). (B, D, and E) Quantified data are expressed as the mean ± SD from three independent biological replicates. Statistical analysis was performed by Student's *t*-test. $*P < 0.05$, $**P < 0.01$, $***P < 0.001$.

2011; Cerutti et al., 2014; Fang et al., 2014). In contrast, SIRT1 protects cardiomyocytes under ischemic stress, exerting suppressive effect on PARP1 activity (Rajamohan et al., 2009). This implies that the hierarchy between PARP1 and SIRT1 changes depending on the physiological context even though the adverse relationships between these proteins persist in diverse disease models. However, it is noteworthy that SIRT1 invariably exerts positive regulatory effects on cell

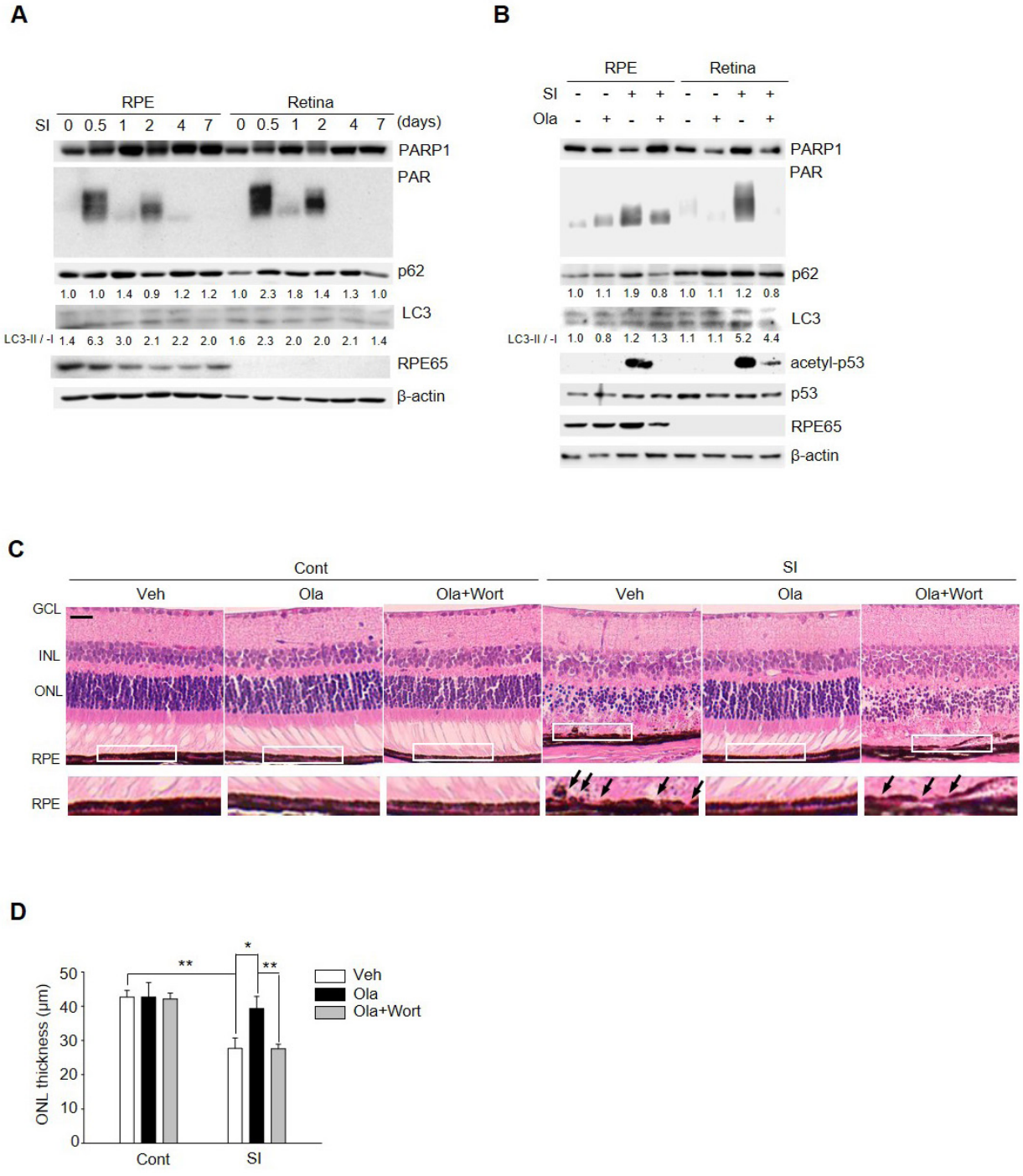

Fig. 5. Autophagy compromise mediated by PARP1 elicits retinal degeneration in a dry AMD mouse. (A) Mice were sacrificed, and lysates of their RPE cells and retinas were analyzed with the indicated antibodies as the indicated days after SI injection. (B) Saline with 10% dimethyl sulfoxide (DMSO) or 15 mg/kg olaparib was administered via intraperitoneal injection. At 30 min after treatment, 30 mg/kg SI was injected into each mouse. At two days after injection, mice were sacrificed, and the retinas were harvested for immunoblot with the indicated antibodies. (A and B) The separated lysates between RPE cells and retinas were analyzed by immunoblotting with anti-RPE65 (marker of RPE cells). The LC3-II/-I ratio and relative p62 levels were quantified by densitometric analyses (ImageJ software). (C and D) Mice were treated with 30 mg/kg SI with or without 15 mg/kg olaparib and 1 mg/kg wortmannin by intraperitoneal injection. At five days after injection, mice were sacrificed and the retinas were harvested for histological analysis using H&E staining. Scale bars = 30 μm. (C) The black arrows indicate representative lesions in damaged RPE area. The graph shows the thickness of the outer nuclear layer (ONL) in H&E-stained samples (n = 6 eyes/group). The thickness was measured using ImageJ software. The values are presented as the mean ± SD from three independent biological replicates. Statistical analysis was performed with Student's *t*-test. $*P < 0.05$, $**P < 0.01$.

survival, whereas PARP1 kills or protects cells depending on the severity of the insult.

The fact that mere NAD^+ supplementation restored SIRT1 activity in H_2O_2-insulted RPE cells implies that NAD^+ mediates SIRT1 inhibition by PARP1. Both PARP1 and SIRT1 utilize NAD^+ for their activities; PARP1 uses PARs converted from NAD^+, and SIRT1 uses NAD^+ as its cofactor (Luna et al., 2013). Interestingly, however, SIRT1, but not PARP1, was influenced by the NAD^+ levels in RPE cells upon H_2O_2 treatment. Indeed, the binding affinity and catalytic activity of PARP1 to NAD^+ are higher than those of SIRT1 (Knight and Chambers, 2001; Smith et al., 2009). Therefore, PARP1 may outcompete SIRT1 for cellular NAD^+, establishing a competitive relationship between PARP1 and SIRT1. Such a superior ability of PARP1 to bind NAD^+ would explain the relative independence of PARP1 on cellular NAD^+ concentration.

PARP1 and SIRT1 play key regulatory roles in mitochondrial homeostasis (Fang et al., 2014). PARP1 impedes mitochondrial functions, while SIRT1 maintains them, in diverse disorders (Bai et al., 2011; Cerutti et al., 2014; Fang et al., 2014). Therefore, manipulation of the PARP1-SIRT1 axis seems to be a plausible strategy for the treatment of mitochondria-related diseases. However, the PARP1 inhibitory drugs on the market target the catalytic activity of PARP1, possibly influencing various biochemical aspects of PARP1. In contrast, a putative compound selectively inhibiting the PARP1-SIRT1 interaction would not exert the unnecessary negative effects on the desirable functions mediated by PARP1. Therefore, the development of a specific inhibitor targeting the PARP1-SIRT1 axis would be beneficial for the treatment of mitochondria-related diseases.

Notably, resveratrol binds to SIRT1 and induces conformational changes to activate SIRT1 (Borra et al., 2005; Cao et al., 2015). Resveratrol-mediated SIRT1 activation has been proven to be beneficial for various disease therapies. For example, resveratrol has been found to attenuate excessive cytokine release to inflammatory neurons in a mouse model of Alzheimer's disease (Chen et al., 2017). In addition, resveratrol sensitizes muscle cells to insulin via SIRT1-mediated mTORC1 inhibition, demonstrating that SIRT1 activation is beneficial for type II diabetes treatment (Kitada and Koya, 2013). Furthermore, resveratrol prevents neuronal loss in multiple sclerosis and encephalomyelitis (Nimmagadda et al., 2013). Given that SIRT1 inactivation is an essential process for RPE degeneration, resveratrol is a plausible therapeutic alternative for dry AMD treatment.

Note: Supplementary information is available on the Molecules and Cells website (www.molcells.org).

ACKNOWLEDGMENTS

This research was supported by a grant of the Korea Health Technology R&D Project through the Korea Health Industry Development Institute (KHIDI), funded by the Ministry of Health & Welfare, Republic of Korea (grant No. HI16C0947).

AUTHOR CONTRIBUTIONS

E.K. and K.H.J. designed all experiments. K.H.J. and Y.H. carried out experiments. E.K. and K.H.J. contributed to the writing of manuscript. All authors contributed to manuscript preparation.

CONFLICT OF INTEREST

The authors have no potential conflicts of interest to disclose.

ORCID

Ki-Hong Jang https://orcid.org/0000-0002-9914-8480
Yeseong Hwang https://orcid.org/0000-0002-1739-4443
Eunhee Kim https://orcid.org/0000-0002-7738-1222

REFERENCES

Abd Elmageed, Z.Y., Naura, A.S., Errami, Y., and Zerfaoui, M. (2012). The poly(ADP-ribose) polymerases (PARPs): new roles in intracellular transport. Cell. Signal. *24*, 1-8.

Bai, P., Canto, C., Oudart, H., Brunyanszki, A., Cen, Y., Thomas, C., Yamamoto, H., Huber, A., Kiss, B., Houtkooper, R.H., et al. (2011). PARP-1 inhibition increases mitochondrial metabolism through SIRT1 activation. Cell Metab. *13*, 461-468.

Borra, M.T., Smith, B.C., and Denu, J.M. (2005). Mechanism of human SIRT1 activation by resveratrol. J. Biol. Chem. *280*, 17187-17195.

Cao, D., Wang, M., Qiu, X., Liu, D., Jiang, H., Yang, N., and Xu, R.M. (2015). Structural basis for allosteric, substrate-dependent stimulation of SIRT1 activity by resveratrol. Genes Dev. *29*, 1316-1325.

Cerutti, R., Pirinen, E., Lamperti, C., Marchet, S., Sauve, A.A., Li, W., Leoni, V., Schon, E.A., Dantzer, F., Auwerx, J., et al. (2014). NAD(+)-dependent activation of Sirt1 corrects the phenotype in a mouse model of mitochondrial disease. Cell Metab. *19*, 1042-1049.

Chang, H.C. and Guarente, L. (2014). SIRT1 and other sirtuins in metabolism. Trends Endocrinol. Metab. *25*, 138-145.

Chen, H., Ji, H., Zhang, M., Liu, Z., Lao, L., Deng, C., Chen, J., and Zhong, G. (2017). An agonist of the protective factor SIRT1 improves functional recovery and promotes neuronal survival by attenuating inflammation after spinal cord injury. J. Neurosci. *37*, 2916-2930.

Cuervo, A.M., Bergamini, E., Brunk, U.T., Droge, W., Ffrench, M., and Terman, A. (2005). Autophagy and aging: the importance of maintaining "clean" cells. Autophagy *1*, 131-140.

David, K.K., Andrabi, S.A., Dawson, T.M., and Dawson, V.L. (2009). Parthanatos, a messenger of death. Front. Biosci. (Landmark Ed.) *14*, 1116-1128.

Fang, E.F., Scheibye-Knudsen, M., Brace, L.E., Kassahun, H., SenGupta, T., Nilsen, H., Mitchell, J.R., Croteau, D.L., and Bohr, V.A. (2014). Defective mitophagy in XPA via PARP-1 hyperactivation and NAD(+)/SIRT1 reduction. Cell *157*, 882-896.

Fatokun, A.A., Dawson, V.L., and Dawson, T.M. (2014). Parthanatos: mitochondrial-linked mechanisms and therapeutic opportunities. Br. J. Pharmacol. *171*, 2000-2016.

Galluzzi, L., Vitale, I., Aaronson, S.A., Abrams, J.M., Adam, D., Agostinis, P., Alnemri, E.S., Altucci, L., Amelio, I., Andrews, D.W., et al. (2018). Molecular mechanisms of cell death: recommendations of the Nomenclature Committee on Cell Death 2018. Cell Death Differ. *25*, 486-541.

Gibson, B.A. and Kraus, W.L. (2012). New insights into the molecular and cellular functions of poly(ADP-ribose) and PARPs. Nat. Rev. Mol. Cell Biol. *13*, 411-424.

Golestaneh, N., Chu, Y., Xiao, Y.Y., Stoleru, G.L., and Theos, A.C. (2017). Dysfunctional autophagy in RPE, a contributing factor in age-related macular degeneration. Cell Death Dis. *8*, e2537.

Govindaraju, V.K., Bodas, M., and Vij, N. (2017). Cigarette smoke induced autophagy-impairment regulates AMD pathogenesis mechanisms in ARPE-19 cells. PLoS One *12*, e0182420.

Hariharan, N., Maejima, Y., Nakae, J., Paik, J., Depinho, R.A., and Sadoshima, J. (2010). Deacetylation of FoxO by Sirt1 plays an essential role in mediating starvation-induced autophagy in cardiac myocytes. Circ. Res. *107*, 1470-1482.

Hu, L., Wang, H., Huang, L., Zhao, Y., and Wang, J. (2016). Crosstalk between autophagy and intracellular radiation response (Review). Int. J. Oncol. *49*, 2217-2226.

Huang, R. and Liu, W. (2015). Identifying an essential role of nuclear LC3 for autophagy. Autophagy *11*, 852-853.

Huang, R., Xu, Y., Wan, W., Shou, X., Qian, J., You, Z., Liu, B., Chang, C., Zhou, T., Lippincott-Schwartz, J., et al. (2015). Deacetylation of nuclear LC3 drives autophagy initiation under starvation. Mol. Cell *57*, 456-466.

Hyttinen, J.M.T., Blasiak, J., Niittykoski, M., Kinnunen, K., Kauppinen, A., Salminen, A., and Kaarniranta, K. (2017). DNA damage response and autophagy in the degeneration of retinal pigment epithelial cells-Implications for age-related macular degeneration (AMD). Ageing Res. Rev. *36*, 64-77.

Imai, S., Armstrong, C.M., Kaeberlein, M., and Guarente, L. (2000). Transcriptional silencing and longevity protein Sir2 is an NAD-dependent histone deacetylase. Nature *403*, 795-800.

Jang, K.H., Do, Y.J., Son, D., Son, E., Choi, J.S., and Kim, E. (2017). AIF-independent parthanatos in the pathogenesis of dry age-related macular degeneration. Cell Death Dis. *8*, e2526.

Kaarniranta, K., Sinha, D., Blasiak, J., Kauppinen, A., Vereb, Z., Salminen, A., Boulton, M.E., and Petrovski, G. (2013). Autophagy and heterophagy dysregulation leads to retinal pigment epithelium dysfunction and development of age-related macular degeneration. Autophagy *9*, 973-984.

Ke, Y., Han, Y., Guo, X., Wen, J., Wang, K., Jiang, X., Tian, X., Ba, X., Boldogh, I., and Zeng, X. (2017). PARP1 promotes gene expression at the post-transcriptiona level by modulating the RNA-binding protein HuR. Nat. Commun. *8*, 14632.

Kiffin, R., Bandyopadhyay, U., and Cuervo, A.M. (2006). Oxidative stress and autophagy. Antioxid. Redox Signal. *8*, 152-162.

Kitada, M. and Koya, D. (2013). SIRT1 in type 2 diabetes: mechanisms and therapeutic potential. Diabetes Metab. J. *37*, 315-325.

Knight, M.I. and Chambers, P.J. (2001). Production, extraction, and purification of human poly(ADP-ribose) polymerase-1 (PARP-1) with high specific activity. Protein Expr. Purif. *23*, 453-458.

Kurz, T., Karlsson, M., Brunk, U.T., Nilsson, S.E., and Frennesson, C. (2009). ARPE-19 retinal pigment epithelial cells are highly resistant to oxidative stress and exercise strict control over their lysosomal redox-active iron. Autophagy *5*, 494-501.

Lee, I.H. (2019). Mechanisms and disease implications of sirtuin-mediated autophagic regulation. Exp. Mol. Med. *51*, 1-11.

Lee, I.H., Cao, L., Mostoslavsky, R., Lombard, D.B., Liu, J., Bruns, N.E., Tsokos, M., Alt, F.W., and Finkel, T. (2008). A role for the NAD-dependent deacetylase Sirt1 in the regulation of autophagy. Proc. Natl. Acad. Sci. U. S. A. *105*, 3374-3379.

Lin, W. and Xu, G. (2019). Autophagy: a role in the apoptosis, survival, inflammation, and development of the retina. Ophthalmic Res. *61*, 65-72.

Luna, A., Aladjem, M.I., and Kohn, K.W. (2013). SIRT1/PARP1 crosstalk: connecting DNA damage and metabolism. Genome Integr. *4*, 6.

Luo, G., Jian, Z., Zhu, Y., Zhu, Y., Chen, B., Ma, R., Tang, F., and Xiao, Y. (2019). Sirt1 promotes autophagy and inhibits apoptosis to protect cardiomyocytes from hypoxic stress. Int. J. Mol. Med. *43*, 2033-2043.

Menzies, F.M., Fleming, A., Caricasole, A., Bento, C.F., Andrews, S.P., Ashkenazi, A., Fullgrabe, J., Jackson, A., Jimenez Sanchez, M., Karabiyik, C., et al. (2017). Autophagy and neurodegeneration: pathogenic mechanisms and therapeutic opportunities. Neuron *93*, 1015-1034.

Mitter, S.K., Song, C., Qi, X., Mao, H., Rao, H., Akin, D., Lewin, A., Grant, M., Dunn, W., Jr., Ding, J., et al. (2014). Dysregulated autophagy in the RPE is associated with increased susceptibility to oxidative stress and AMD. Autophagy *10*, 1989-2005.

Nah, J., Yuan, J., and Jung, Y.K. (2015). Autophagy in neurodegenerative diseases: from mechanism to therapeutic approach. Mol. Cells *38*, 381-389.

Navarro-Yepes, J., Burns, M., Anandhan, A., Khalimonchuk, O., del Razo, L.M., Quintanilla-Vega, B., Pappa, A., Panayiotidis, M.I., and Franco, R. (2014). Oxidative stress, redox signaling, and autophagy: cell death versus survival. Antioxid. Redox Signal. *21*, 66-85.

Nimmagadda, V.K., Bever, C.T., Vattikunta, N.R., Talat, S., Ahmad, V., Nagalla, N.K., Trisler, D., Judge, S.I., Royal, W., 3rd, Chandrasekaran, K., et al. (2013). Overexpression of SIRT1 protein in neurons protects against experimental autoimmune encephalomyelitis through activation of multiple SIRT1 targets. J. Immunol. *190*, 4595-4607.

Ohsumi, Y. (2001). Molecular dissection of autophagy: two ubiquitin-like systems. Nat. Rev. Mol. Cell Biol. *2*, 211-216.

Rajamohan, S.B., Pillai, V.B., Gupta, M., Sundaresan, N.R., Birukov, K.G., Samant, S., Hottiger, M.O., and Gupta, M.P. (2009). SIRT1 promotes cell survival under stress by deacetylation-dependent deactivation of poly(ADP-ribose) polymerase 1. Mol. Cell. Biol. *29*, 4116-4129.

Rodriguez-Vargas, J.M., Oliver-Pozo, F.J., and Dantzer, F. (2019). PARP1 and poly(ADP-ribosyl)ation signaling during autophagy in response to nutrient deprivation. Oxid. Med. Cell. Longev. *2019*, 2641712.

Rodriguez-Vargas, J.M., Rodriguez, M.I., Majuelos-Melguizo, J., Garcia-Diaz, A., Gonzalez-Flores, A., Lopez-Rivas, A., Virag, L., Illuzzi, G., Schreiber, V., Dantzer, F., et al. (2016). Autophagy requires poly(adp-ribosyl)ation-dependent AMPK nuclear export. Cell Death Differ. *23*, 2007-2018.

Rubinsztein, D.C., Marino, G., and Kroemer, G. (2011). Autophagy and aging. Cell *146*, 682-695.

Ryter, S.W., Cloonan, S.M., and Choi, A.M. (2013). Autophagy: a critical regulator of cellular metabolism and homeostasis. Mol. Cells *36*, 7-16.

Salminen, A. and Kaarniranta, K. (2009). SIRT1: regulation of longevity via autophagy. Cell. Signal. *21*, 1356-1360.

Smith, B.C., Hallows, W.C., and Denu, J.M. (2009). A continuous microplate assay for sirtuins and nicotinamide-producing enzymes. Anal. Biochem. *394*, 101-109.

Wang, C., Xu, W., Zhang, Y., Zhang, F., and Huang, K. (2018). PARP1 promote autophagy in cardiomyocytes via modulating FoxO3a transcription. Cell Death Dis. *9*, 1047.

Wang, Y., Kim, N.S., Haince, J.F., Kang, H.C., David, K.K., Andrabi, S.A., Poirier, G.G., Dawson, V.L., and Dawson, T.M. (2011). Poly(ADP-ribose) (PAR) binding to apoptosis-inducing factor is critical for PAR polymerase-1-dependent cell death (parthanatos). Sci. Signal. *4*, ra20.

Wei, H., Xun, Z., Granado, H., Wu, A., and Handa, J.T. (2016). An easy, rapid method to isolate RPE cell protein from the mouse eye. Exp. Eye Res. *145*, 450-455.

Wu, Y., Li, X., Zhu, J.X., Xie, W., Le, W., Fan, Z., Jankovic, J., and Pan, T. (2011). Resveratrol-activated AMPK/SIRT1/autophagy in cellular models of Parkinson's disease. Neurosignals *19*, 163-174.

Wyrsch, P., Blenn, C., Bader, J., and Althaus, F.R. (2012). Cell death and autophagy under oxidative stress: roles of poly(ADP-Ribose) polymerases and Ca(2+). Mol. Cell. Biol. *32*, 3541-3553.

Yetimakman, A.F., Oztarhan, K., and Aydogan, G. (2014). Comparison of tissue Doppler imaging with MRI t2* and 24-hour rhythm holter heart rate variability for diagnosing early cardiac impairment in thalassemia major patients. Pediatr. Hematol. Oncol. *31*, 597-606.

Yoshii, S.R. and Mizushima, N. (2017). Monitoring and measuring autophagy. Int. J. Mol. Sci. *18*, 1865.